Nanostructure Templating in Inorganic Solids with Organic Lyotropic Liquid Crystals

Paul V. Braun, Paul Osenar, Valeria Tohver, Scott B. Kennedy, and Samuel I. Stupp*

Contribution from the Departments of Materials Science and Engineering and Chemistry, Northwestern University, Evanston, Illinois 60208

Received September 21, 1998. Revised Manuscript Received April 21, 1999

Abstract: Various nanoscale semiconducting superlattices have been generated by direct templating in a lyotropic organic liquid crystal. These include superlattices of CdS, CdSe, and ZnS, templated in a liquid crystal formed by oligoethylene oxide oleyl ether amphiphiles and water. The semiconductor growth process copied the symmetry and characteristic dimensions of the original mesophase by avoiding growth of mineral within regularly spaced hydrophobic regions. The final product was a superlattice structure in which a mineral continuum was featured with hexagonally arranged cylindrical pores 2−3 nm in diameter and 5 nm apart. Most importantly, the superlattice morphology of the nanostructured systems in contact with the mesophase was found to be thermodynamically stable with respect to the solid lacking nanoscale features. We also found that both the morphology of features in the nanostructured solids and their dimension can be controlled through the amphiphile's molecular structure and water content in the liquid crystal. The semiconducting solids CdS, CdSe, and ZnS were all directly templated, while Ag_2S, CuS, HgS, and PbS were produced only as nonfeatured solids using identical synthetic methodologies. We propose that interactions of polar segments in template molecules with the precipitated mineral and with its precursor ions are necessary conditions for direct templating. This is based on the absence of templating in the more covalent minerals and also in the presence of salts known to bind precursor ions.

Introduction

The synthesis of solids with defined nanometer scale features is of great interest in materials chemistry. There has been a significant effort to generate nanostructured materials with techniques ranging from scanning microscopies to molecular self-assembly.[1−9] Careful control of molecular architecture can yield many different nanostructured organics. The mineralization and polymerization of these organized systems can contribute further to the design of novel solid-state structures. For example, mineral growth within and on lipid aggregates has resulted in unusual morphologies including mineralized tubules and disks.[10,11] A recent approach to controlling mineral growth through self-assembly involves the co-assembly of molecular species and mineral phase precursors into nanoporous structures. This methodology has been quite successful in the formation of a variety of mesoporous oxides.[12−18] Our objective here has been to utilize the order present in an organic mesophase to template *directly* the growth of an inorganic phase. The growth of minerals in a preformed liquid crystal has been attempted, but prior to our work, only oblong or cubic crystallites or microporous reticulated structures had been obtained.[19−21] Our work represents the first successful templated synthesis of periodically nanostructured inorganics which copied directly the symmetry and dimensionality of the organic precursor.[6,22−25]

* To whom correspondence should be addressed. This work was carried out at the University of Illinois at Urbana-Champaign.

(1) Stroscio, J. A.; Eigler, D. M. *Science* **1991**, *254*, 1319.
(2) Whitesides, G. M.; Mathias, J. P.; Seto, C. T. *Science* **1991**, *254*, 1312.
(3) Mann, S.; Ozin, G. A. *Nature* **1996**, *382*, 313.
(4) Special Issue on Nanostructures. *Chem. Mater.* **1996**, *8*, 1569.
(5) Stupp, S. I.; LeBonheur, V.; Walker, K.; Li, L. S.; Huggins, K. E.; Keser, M.; Amstutz, A. *Science* **1997**, *276*, 384.
(6) Stupp, S. I.; Braun, P. V. *Science* **1997**, *277*, 1242.
(7) Liu, J.; Kim, A. Y.; Wang, L. Q.; Palmer, B. J.; Chen, Y. L.; Bruinsma, P.; Bunker, B. C.; Exarhos, G. J.; Graff, G. L.; Rieke, P. C.; Fryxell, G. E.; Virden, J. W.; Tarasevich, B. J.; Chick, L. A. *Adv. Colloid Interface Sci.* **1996**, *69*, 131.
(8) Shenton, W.; Pum, D.; Sleytr, U. B.; Mann, S. *Nature* **1997**, *389*, 585.
(9) Neeraj; Rao, C. N. R. *J. Mater. Chem.* **1998**, *8*, 279.
(10) Schnur, J. M. *Science* **1993**, *262*, 1669.
(11) Archibald, D. D.; Mann, S. *Nature* **1993**, *364*, 430.
(12) Kresge, C. T.; Leonowicz, M. E.; Roth, W. J.; Vartuli, J. C.; Beck, J. S. *Nature* **1992**, *359*, 710.
(13) Beck, J. S.; Vartuli, J. C.; Kennedy, G. J.; Kresge, C. T.; Roth, W. J.; Schramm, S. E. *Chem. Mater.* **1994**, *6*, 1816.
(14) Monnier, A.; Schuth, F.; Huo, Q.; Kumar, D.; Margolese, D.; Maxwell, R. S.; Stucky, G. D.; Krishnamurty, M.; Petroff, P.; Firouzi, A.; Janicke, M.; Chmelka, B. F. *Science* **1993**, *261*, 1299.
(15) Huo, Q.; Margolese, D. I.; Ciesla, U.; Feng, P.; Gier, T. E.; Sieger, P.; Leon, R.; Petroff, P. M.; Schuth, F.; Stucky, G. D. *Nature* **1994**, *368*, 317.
(16) Firouzi, A.; Kumar, D.; Bull, L. M.; Besier, T.; Sieger, P.; Huo, Q.; Walker, S. A.; Zasadzinski, J. A.; Glinka, C.; Nicol, J.; Margolese, D.; Stucky, G. D.; Chmelka, B. F. *Science* **1995**, *267*, 1138.
(17) Attard, G. S.; Glyde, J. C.; Goltner, C. R. *Nature* **1995**, *378*, 366.
(18) Beck, J. S.; Vartuli, J. C. *Curr. Opin. Solid State Mater. Sci.* **1996**, *1*, 76.
(19) Fribreg, S. E.; Wang, J. *J. Dispersion Sci. Technol.* **1991**, *12*, 387.
(20) Walsh, D.; Hopwood, J. D.; Mann, S. *Science* **1994**, *264*, 1576.
(21) Yang, J. P.; Qadri, S. B.; Ratna, B. R. *J. Phys. Chem.* **1996**, *100*, 17255.
(22) Braun, P. V.; Osenar, P.; Stupp, S. I. *Nature* **1996**, *380*, 325.
(23) Osenar, P.; Braun, P. V.; Stupp, S. I. *Adv. Mater.* **1996**, *8*, 1022.
(24) Tohver, V.; Braun, P. V.; Pralle, M. U.; Stupp, S. I. *Chem. Mater.* **1997**, *9*, 1495.
(25) Braun, P. V.; Stupp, S. I. *Mater. Res. Bull.* **1999**, *23*, 463.
(26) Attard, G. S.; Bartlett, P. N.; Coleman, N. R. B.; Elliott, J. M.; Owen, J. R.; Wang, J. H. *Science* **1997**, *278*, 838.
(27) Attard, G. S.; Edgar, M.; Goltner, C. G. *Acta Materialia* **1998**, *46*, 751.

10.1021/ja9833725 CCC: $18.00
Published on Web 07/29/1999

The liquid crystal templating of periodically nanostructured metals, both as thin films and in bulk, was also reported recently.[26,27]

The synthesis of II−VI semiconductor particles and films has been studied for some time due to their technologically important properties. The study of small particles has been of significant interest since their properties change drastically as the nanoscale regime is approached.[28−30] In this context, the synthetic methodologies for the formation of metal sulfide and selenide quantum dots and their assembly into higher-order structures have been widely studied.[31−35] Despite the large volume of work in this area, all of the systems studied have produced solid semiconductor particles with morphologies never far from spherical. The possibility of generating complicated morphologies can be observed in studies of CdS synthesized under Langmuir monolayers, where dendritic structures have been observed.[36] However, the emphasis in the past has been on growing nanocrystals with narrow size distributions, and not superlattice structures. In one case CdSe nanocrystals were observed to order into a superlattice structure through careful control of size distribution and chemical functionality.[33] The individual crystallites in this system do not form a continuous mineral structure but are separated by thin organic regions.

Our work involves the direct templating of CdS as well as other semiconducting solids in the preordered environment of a nonionic amphiphilic mesophase, generating semiconductor-organic superlattices containing both the symmetry and long-range order of the precursor liquid crystal. The semiconductor is grown in a water-containing liquid crystal by the reaction of H_2S or H_2Se with a dissolved salt. Through this work we have shown the importance of both chemical nature and structure of the amphiphile in direct templating. In fact, the order obtained in the nanostructured systems was even found to be dependent on the anion of the salt.[24] The direct templating process opens up a variety of synthetic avenues to the formation of novel nanostructures. There are a large number of amphiphilic liquid crystals, with lattice constants ranging from a few nanometers to tens of nanometers, which include lamellar, hexagonal, cubic, and bicontinuous phases.[37−39] Potentially, many of these systems could be mineralized, generating materials with an array of novel structures and properties.

An exciting possibility is the use of templating methodologies to intimately disperse functionalized organic molecules in inorganic lattices. Inorganic solids containing molecularly dispersed organic molecules could form composite materials with novel properties and structures significantly enhanced over those of either the inorganic or organic phase alone.[40] These composite materials may be tougher,[41−43] have increased thermal stability,[44] be electronically more sophisticated,[45,46] or have enhanced chemical selectivity[47] than either of the constituent parts. Even without the incorporation of organic material, periodically nanostructured semiconductors have great potential in solid-state science and technology as electronically and catalytically active materials. For example, a periodically activated semiconductor might behave as an array of antidots, a material with a regular array of scattering centers spaced closer than the mean free path of electrons traveling through them.[48,49] As opposed to the quantum dots previously mentioned, the formation of an antidot lattice requires the semiconducting structures to be continuous. The ability to define a periodic array of nanocavities in a semiconducting material would also open up a host of opportunities for catalytic and photonic materials. The thermal stability of the nanostructured superlattices combined with their electronic and photonic properties could lead to highly functional materials. Furthermore, templating methodologies could afford molecularly modified semiconductors.

Results and Discussion

It is quite remarkable that a soft organic liquid crystal could directly template a hard covalent mineral phase. As we first demonstrated, the hexagonal mesophase formed by 50 vol % aqueous 0.1 M $Cd(OAc)_2$ and 50 vol % oligoethylene oxide ($\overline{10}$) oleyl ether [$(EO)_{\overline{10}}$oleyl] templated an inorganic−organic nanocomposite of CdS and amphiphile when exposed to H_2S gas.[22] The composite material synthesized contained an internal nanostructure replicating the symmetry and dimensions of the liquid crystal in which it was grown. The $(EO)_{\overline{10}}$oleyl system is quite versatile when combined with H_2O, forming a hexagonal mesophase at 25 °C over the composition range of ∼35−65 vol % amphiphile, and a lamellar mesophase from ∼70 to 85 vol % amphiphile.[50,51] Polarized optical microscopy (POM) was used to verify the phase diagram, and the textures were consistent with those published for these mesophases.[38] In an effort to understand further the templating phenomenon, we grew several other sulfides and selenides from their respective salts within various amphiphilic mesophases, all of which were based on $(EO)_{\overline{10}}$oleyl. CdS and ZnS particles were found to exhibit the periodic porosity, while Ag_2S, CuS, HgS, and PbS did not exhibit this superlattice morphology (see Figure 1 for examples). CdSe is also nanostructured, although due to difficulties in the synthesis, many of the particles did not exhibit the superlattice morphology. Presumably under more controlled conditions CdSe would behave similarly to CdS and ZnS. The

(28) Weller, H. *Angew. Chem., Int. Ed. Engl.* **1993**, *32*, 41.
(29) Weller, H. *Adv. Mater.* **1993**, *5*, 88.
(30) Weller, H. *Philos. Trans. R. Soc. London A* **1996**, *354*, 757.
(31) Murray, C. B.; Norris, D. J.; Bawendi, M. G. *J. Am. Chem. Soc.* **1993**, *115*, 8706.
(32) Dabbousi, B. O.; Murray, C. B.; Rubner, M. F.; Bawendi, M. G. *Chem. Mater.* **1994**, *6*, 216.
(33) Murray, C. B.; Kagan, C. R.; Bawendi, M. G. *Science* **1995**, *270*, 1335.
(34) Alivisatos, A. P. *MRS Bull.* **1995**, *20*, 23.
(35) Peng, X.; Wilson, T. E.; Alivisatos, A. P.; Schultz, P. G. *Angew. Chem., Int. Ed. Engl.* **1997**, *36*, 145.
(36) Fendler, J. H. *Membrane-Mimetic Approach to Advanced Materials*; Springer-Verlag: Berlin, Germany, 1994.
(37) Schick, M. J. *Nonionic Surfactants, Physical Chemistry*; Marcel Dekker: New York, 1987.
(38) Laughlin, R. G. *The Aqueous Phase Behavior of Surfactants*; Academic Press Inc.: San Diego, CA, 1994.
(39) Wanka, G.; Hoffmann, H.; Ulbricht, W. *Macromolecules* **1994**, *27*, 4145.
(40) Messersmith, P. B.; Stupp, S. I. *J. Mater. Res.* **1992**, *7*, 2599.
(41) Berman, A.; Addadi, L.; Weiner, S. *Nature* **1988**, *331*, 546.
(42) Berman, A.; Addadi, L.; Kvick, Å.; Leiserowitz, L.; Nelson, M.; Weiner, S. *Science* **1990**, *250*, 664.
(43) Berman, A.; Hanson, J.; Leiserowitz, L.; Koetzle, T. F.; Weiner, S.; Addadi, L. *Science* **1993**, *259*, 776.
(44) Messersmith, P. B.; Stupp, S. I. *Chem. Mater.* **1995**, *7*, 454.
(45) Mitzi, D. B.; Feild, C. A.; Harrison, W. T. A.; Guloy, A. M. *Nature* **1994**, *369*, 467.
(46) Mitzi, D. B.; Wang, S.; Feild, C. A.; Chess, C. A.; Guloy, A. M. *Science* **1995**, *267*, 1473.
(47) Feng, X.; Fryxell, G. E.; Wang, Q.-L.; Kim, A. Y.; Liu, J.; Kemner, K. M. *Science* **1997**, *276*, 923.
(48) Weiss, D.; Roukes, M. L.; Mensching, A.; Grambow, P.; Klitzing, K. v.; Weimann, G. *Phys. Rev. Lett.* **1991**, *66*, 2790.
(49) Hansen, W.; Kotthaus, J. P.; Merkt, U. *Electrons in Laterally Periodic Nanostructures*; Hansen, W., Kotthaus, J. P., Merkt, U., Eds.; Academic Press, 1992; Vol. 35, p 279.
(50) Lo, I.; Florence, A. T.; Treguier, J.-P.; Seiller, M.; Puisieux, F. *J. Colloid Interface Sci.* **1977**, *59*, 319.
(51) Treguier, J. P.; Seiller, M.; Puisieux, F.; Orecchioni, A. M.; Florence, A. T. *Effect of a hydrophilic surfactant and temperature on water−surfactant-oil diagrams*; Treguier, J. P., Seiller, M., Puisieux, F., Orecchioni, A. M., Florence, A. T., Eds.; Assoc. Pharm., 1977; Vol. 1, p 75.

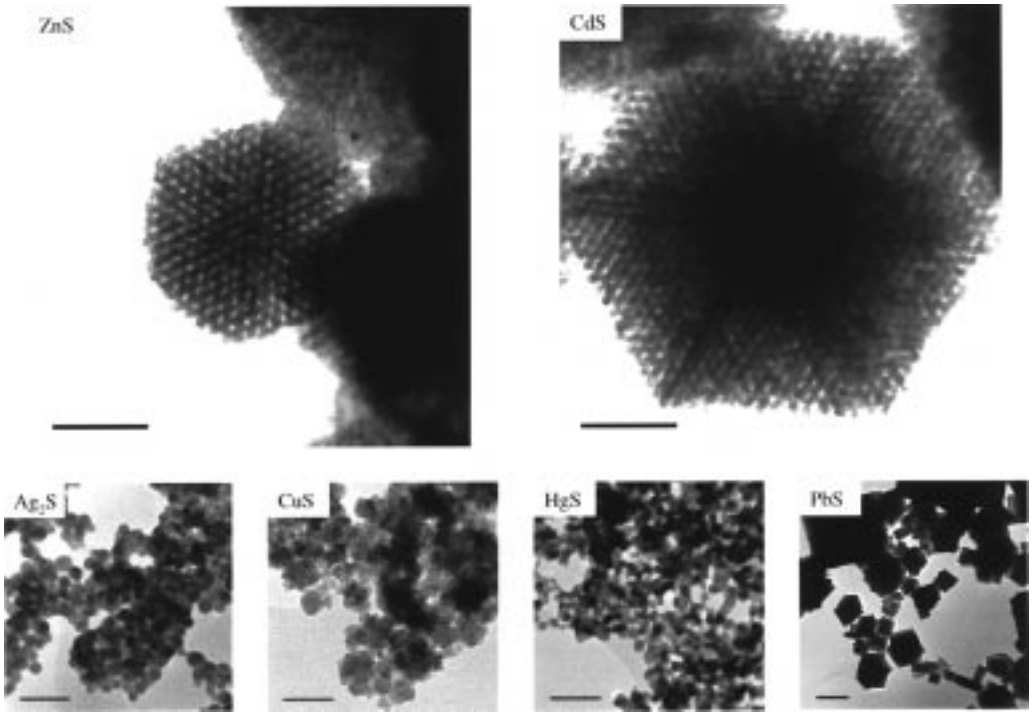

Figure 1. TEM images of mineralized structures grown in hexagonal mesophases from their respective nitrate salt and H_2S (bar = 50 nm except, for PbS, bar = 250 nm).

precipitation of CoS and NiS via a similar methodology was also attempted, and no periodic structure was observed. Upon exposure to moisture these minerals convert to Co(OH)S and Ni(OH)S,[52] respectively, and so were not studied further. The CdS and ZnS superlattice structures were quite stable to removal of the amphiphile. Even after being heated to 350 °C in air, their nanostructured morphology remained unchanged.

Direct templating of an inorganic solid by an organic liquid crystal may depend on many factors, but we propose that the thermodynamic stability of the mesophase throughout the mineral growth process is an important element. First of all, it was necessary to prove that the addition of ions and the mineral precipitation process did not disrupt the order of the liquid crystal. This is a necessary condition to define the synthesis as *direct templating*. The textures observed in POM did not change when any of the 0.01−0.1 M salt solutions were substituted for pure water in forming the mesophase, indicating that ionic doping of aqueous compartments did not disrupt order extensively in the mesophase. To further verify that the characteristic molecular order of the mesophase was not disrupted by ion doping, we obtained broadline ^{2}H NMR spectra from both doped and undoped mesophases. For both mesophases, the same quadrupolar splitting was observed (Figure 2). If ionic doping had perturbed the structure of the mesophase, the splitting would have decreased.[53,54] As additional proof of molecular order in the mesophase, X-ray diffractograms were collected to characterize both the mesophase's long period and symmetry. For systems containing 35%, 40%, 50%, and 60% amphiphile, the 100, 110, and 200 reflections are clearly observed, indicating that the liquid crystalline structure is hexagonal (Figure 3). A mesophase containing 78% amphiphile forms a lamellar liquid crystal as indicated by the 001 and 002 reflections and absence of the 110 reflection (Figure 4). As expected, we found a strong correlation between the phase diagrams as determined by POM and X-ray diffraction. Precipitation of mineral particles within these systems also causes little disruption as determined by X-ray diffraction or POM.[22] For successful direct templating it is important that the liquid crystal is stable at all stages of the templating process. For example, when the $(EO)_{\overline{10}}$oleyl-based mesophases were disrupted by doping with 0.5 M aqueous salts, the minerals grown in these systems did not exhibit the superlattice morphology.

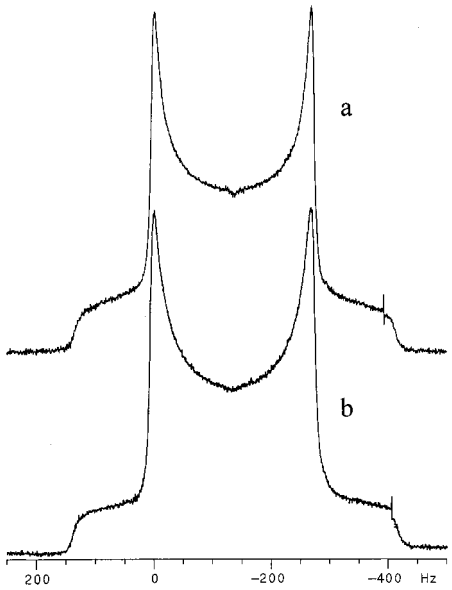

Figure 2. Quadrupolar splitting for a hexagonal mesophase doped with 0.1 M $Cd(OAc)_2$ (a) and for an undoped hexagonal mesophase (b).

To further verify the direct templating nature of precipitation within the mesophase, we mineralized samples composed of 35, 40, 50 and 60 wt % $(EO)_{\overline{10}}$oleyl with CdS. On the basis of the assumption that the CdS is directly templated by the liquid crystal in which it is grown, the hexagonal symmetry and associated periodicity should be nearly identical to those found

(52) Cotton, F. A.; Wilkinson, G. *Advanced Inorganic Chemistry*, 5th ed.; Cotton, F. A., Wilkinson, G., Eds.; John Wiley & Sons: New York, 1988; p 605.

(53) Blackburn, J. C.; Kilpatrick, P. K. *Langmuir* **1992**, *8*, 1679.

(54) Schnepp, W.; Disch, S.; Schmidt, C. *Liq. Cryst.* **1993**, *14*, 843.

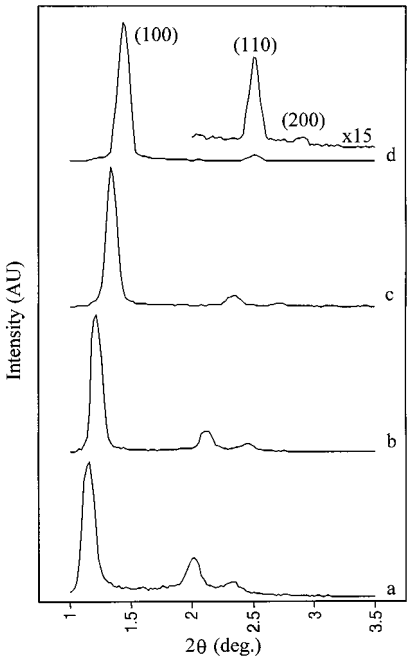

Figure 3. X-ray diffraction scan of hexagonal aqueous mesophases containing (a) 35%, (b) 40%, (c) 50%, and (d) 60% amphiphile by volume.

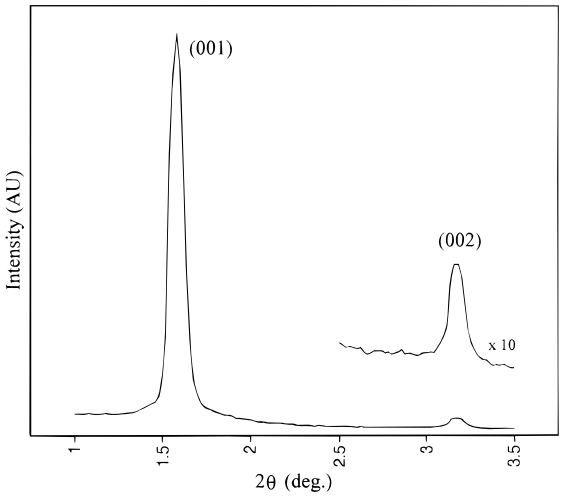

Figure 4. X-ray diffraction of lamellar mesophase containing 78% amphiphile and 22% water by volume.

in the precursor hexagonal mesophase. By varying the amphiphile content of the mesophase, we observed the expected variation of the spacing between the hexagonally packed cylindrical aggregates of amphiphilic molecules. Figure 5 shows the center to center distance between cavities in the mineralized structure as measured by TEM and also the center to center distance between hydrophobic cores in the precursor mesophases as measured by SAXS (undoped with metal ions). The diffraction peaks were quite sharp, and thus error bars were not assigned to the calculated spacings. As shown in the figure, the variation of spacings observed by TEM in the mineralized structures was about ±0.5 nm. The observed correlation between superlattice dimension in the precipitate and the mesophase's lattice constant offers very strong evidence for direct templating. If the superlattice dimension of the precipitate had not changed with the lattice constant of the templating mesophase, it could be argued that the superlattice is generated not by direct templating but via a co-assembly process much as is hypothesized to be the case in the mesoporous oxide synthesis.[14,16]

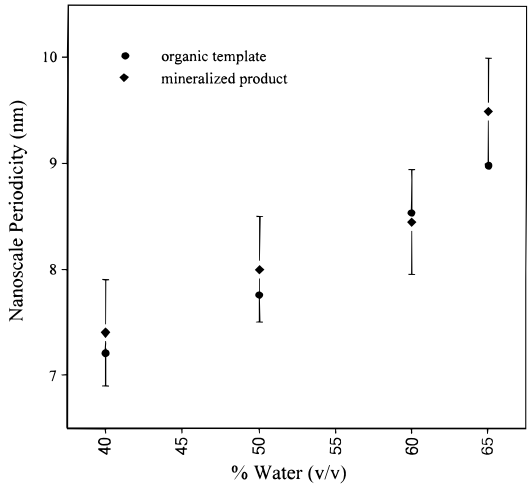

Figure 5. Center to center spacing in the cylindrical assemblies of amphiphilic molecules of hexagonal mesophases determined by X-ray diffraction scans in Figure 3 (●), and center to center pore spacing in templated solids as measured by TEM (◆), both as a function of water content in the mesophase.

As shown in Figure 1, the nanostructures of the semiconductors CdS and ZnS synthesized by precipitation in hexagonal mesophases doped with their respective nitrate salts have hexagonal symmetry with a periodicity commensurate with that of the template. The hexagonal nanostructure is not always evident in TEM micrographs as a result of random orientation of particles in the field of view. For this reason, only a small percentage of the particles reveal their hexagonal symmetry, yet the vast majority are templated. This can be demonstrated by tilting the samples in the TEM stage, revealing many more particles with hexagonal nanostructure. Tilting of the sample in the TEM stage confirms that the templated particles are generally spherical, although occasionally a particle may exhibit some degree of faceting. As previously reported, CdS is also periodically nanostructured when grown from the acetate salt, but order in the nanostructured solid is not nearly as high as in the nitrate-derived systems.[24] When ZnS is synthesized from its acetate salt, only spherical polycrystalline particles with a porous appearance are formed. Another difference between the product obtained from the acetate and nitrate salts is the average particle diameters of the semiconductor product. Both CdS and ZnS particles grown from their respective nitrate salts were approximately five times larger than those grown from the acetate salts. This size difference can be clearly observed in low magnification electron micrographs. CdS was also grown in aqueous environments from both the nitrate and acetate precursors, and as expected nanostructures were not observed in these control samples. The counterion of the metal did not have any effect on the nature of the product obtained in Ag_2S, CuS, HgS, and PbS samples. A superlattice morphology was not observed in any of these sulfides formed in the hexagonal mesophase from either acetate or nitrate salts.

It is interesting to consider the differences in product morphologies between the acetate and nitrate systems. As previously mentioned, CdS and ZnS can be grown from either their acetate or nitrate salts, but the average particle diameter and degree of order in the nanostructure are strongly affected by the nature of the anion of the precursor metal salt. We believe the rates of diffusion, and thus nucleation and growth, are similar for both the acetate and nitrate systems. Therefore, the large increase in the average particle diameter observed in the nitrate case is most likely due to a ripening process. In the acetate systems, the byproduct (acetic acid) cannot significantly dissolve

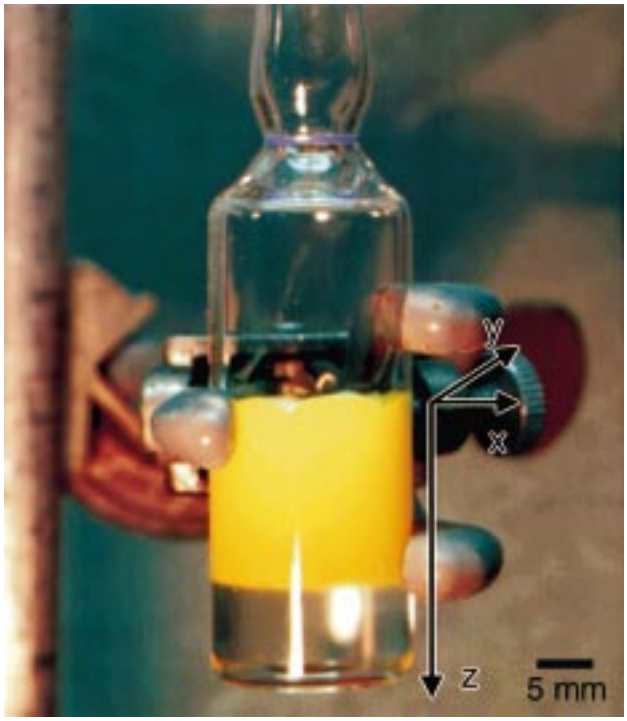

Figure 6. CdS mineralization of the $Cd(NO_3)_2$ doped hexagonal mesophase after 24 h of H_2S exposure. The hydrated H_2S enters the clear gel formed by the hexagonal mesophase from the top of the vial, and the opaque medium shows the z-position of the mineralization front.

the sulfides and thus particle coarsening is not expected (reaction 1). Conversely, in the nitrate systems, the acid byproduct (nitric acid) dissolves the sulfide, thus allowing Ostwald ripening through the back reaction shown in reaction 2,

$$M(OAc)_2 + H_2S \rightleftharpoons MS + 2HOAc \quad (1)$$

$$M(NO_3)_2 + H_2S \rightleftharpoons MS + 2HNO_3 \quad (2)$$

However, the high concentration of H_2S gas dissolved in the mesophase after the precipitation reaction is complete makes the back reactions rather unfavorable. For this reason, ripening only occurs in the nitrate systems before the mesophase becomes saturated with H_2S. Once the mesophase is saturated with H_2S, even reaction 2 is driven far to the right, reducing essentially to zero the concentration of free metal ions necessary for ripening.

Strong evidence for Ostwald ripening was obtained by harvesting the particles formed at different stages of the reaction. Because all of the H_2S must enter the mesophase at the air−mesophase interface, the CdS closest to this interface is produced first (z-coordinate equals zero) and progressively later with increasing z-coordinate. Figure 6 is an actual picture of a partially mineralized mesophase after 24 h of H_2S exposure. The H_2S has not yet diffused to the bottom of the templating gel, so that region remains clear. TEM images of the top 2 mm layer showed many morphologically unordered 20 nm particles and relatively few ordered particles ranging in size from 0.1 to 2 μm. The next layer (2−4 mm deep) contained 0.1−3 μm nanostructured particles. The layers 4−10 mm away from the air mesophase interface contained nanostructured particles 0.5−5 μm in diameter, and the last layer, corresponding to a depth of 10−12 mm from the interface, contained nanostructured particles ranging from 0.5 to 7.5 μm. Any layers deeper than 12 mm had not yet been exposed to H_2S gas and thus contained

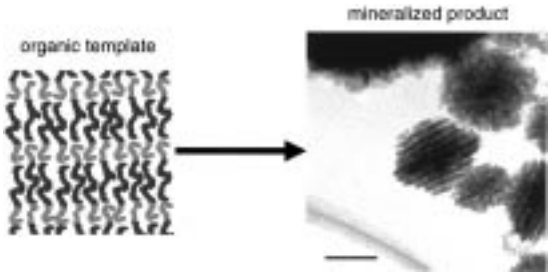

Figure 7. Schematic representation of the lamellar organic template and TEM image of the resulting product after mineralization (bar = 50 nm). The dark regions of the schematic contain the oligoethylene oxide segments of the template, and the oleyl segments populate the light regions.

no precipitate. At the top of the mesophase, the very small average particle size seems to indicate that the initial saturation of H_2S in this layer leads to rapid nucleation. Although the H_2S favors the formation of CdS and the nitric acid byproduct, the rapid saturation of the mesophase also limits the concentration of free cadmium ions available for ripening, leading mostly to small particles. Further away from the mesophase−air interface, a significant time elapses between the first precipitation of CdS and complete saturation of the mesophase with H_2S. During this time, the lower concentration of H_2S leads to more free metal ions and thus Ostwald ripening. In principle, these free ions could nucleate new particles, but growth of larger particles appears to be more energetically favorable. The time between this initial precipitation and the termination of Ostwald ripening (due to H_2S saturation) increases away from the mesophase−air interface. We propose this explains why the average particle diameter increases away from the air interface in the reaction medium. Further support to the ripening effect is offered by the same experiment but using $Cd(OAc)_2$ as opposed to $Cd(NO_3)_2$. In this case, very little difference was observed in the size of the particles formed as a function of z-coordinate.

As discussed above, when CdS or ZnS is grown from their respective nitrate salts, the byproduct of the reaction is a strong acid, leading to ripening. Since nitrate salts yield the best copy of the organic template even though ripening occurs, the periodically nanostructured system appears to be thermodynamically stable relative to nonfeatured CdS or ZnS in contact with the mesophase. Presumably, the presence of nitric acid allows for the dissolution of high-energy particles and the growth of others lower in energy. Interestingly, when the initial concentration of $Cd(NO_3)_2$ was 0.025 M, the order observed in the particles was not as sharp as that observed when using a concentration of 0.1 M $Cd(NO_3)_2$. Perhaps this is due to the lower concentration of nitric acid byproduct, which reduces the ability of the system to access its low-energy morphology. The thermodynamic stability of the nanostructured systems is also demonstrated by comparing ZnS produced from $Zn(NO_3)_2$ versus that generated from $Zn(OAc)_2$. The acetate preparation results in particles which appear somewhat porous but without a periodic nanostructure; however, as shown in Figure 1, the nitrate system yields significantly larger particles containing a very well-defined superlattice. Apparently, ZnS generated from the acetate is kinetically trapped without a superlattice structure.

In addition to the hexagonal mesophase, a lamellar mesophase of $(EO)_{\overline{10}}$oleyl also has the ability to template directly a precipitated mineral (Figure 7). The lamellar periodicity observed in the resulting CdS is ∼7 nm, which matches fairly well the periodicity of the lamellar organic template. The lamellar morphology can be confirmed by tilting particles in the TEM. The image remains unchanged when particles are

tilted about an axis perpendicular to the stripes. However, the periodic pattern quickly vanishes when tilting about an axis parallel to the stripes and perpendicular to the electron beam. This difference was observed in experimental samples, offering strong evidence for a lamellar morphology within the particles. Interestingly, particles containing the lamellar morphology are stable to repeated sonication, perhaps due to bridging between CdS layers by anchored molecules. Alternatively, CdS could nucleate within a hydrophilic layer of the mesophase and grow rapidly in the plane but occasionally form a finger perpendicular to this layer, piercing the hydrophobic region. This finger then nucleates another layer of CdS, resulting in a mineral bridge between layers. Of course growth in the plane of the layers is faster than that perpendicular to the layers, generating the disk like habit observed. Not surprisingly, the lamellar CdS was only observed when the nitrate salt was used, while 0.1 M $Cd(OAc)_2$ afforded only small particles.

In an effort to further elucidate the mechanism for the formation of the superlattice structures, we also considered the interaction of various precursor ions with the mesophase. These included the binding of Cd^{2+} ions with either nitrilotriacetic acid trisodium salt (NaNTA) or NH_3 (known Cd^{2+} binders[55,56]) followed by precipitation of CdS and the measurement of relative rates of diffusion for Cd^{2+} and Pb^{2+} ions in the mesophase. The system containing NaNTA affords CdS particles of approximately the same size as those generated without it (for both the acetate and nitrate systems), but a periodic nanostructure is not observed (see Figure 8). On the other hand, CdS grown in the presence of NH_3 consisted exclusively of small, solid particles, again with no periodic morphology. These results indicate that oligoethylene oxide−cation interactions do play some role in the mesophase templating phenomenon. If confinement of the reactive species to the hydrophilic region of the mesophase was the sole driving force for nanostructure formation, templating would be expected in these systems since the cadmium species bound by NaNTA or NH_3 are still quite polar and are certainly confined to the hydrophilic region of the mesophase. To investigate further the importance of the hydrophile−metal ion interaction, we measured the relative diffusion rates of Cd^{2+} and Pb^{2+}. In the diffusion experiment, both CdS and PbS started precipitating 6 h after the H_2S gas flow was started, approximately 3 mm above the original undoped−doped interface, suggesting that the rates of diffusion in the mesophase for both ions are similar. Using the diffusion equation, $x = 2\sqrt{Dt}$, and the above data, the diffusion coefficient (D) of both ions in the mesophase is calculated to be $\sim 1 \times 10^{-6}$ cm^2/s, which is only about a factor of 10 less than the diffusion coefficient of the salts in pure water.[57,58] The similar mobility of the lead and cadmium salts in water and in the aqueous based mesophase indicates that strong oligoethylene oxide−cation complexes are not formed, which agrees with previous work on the interaction of Pb^{2+}, Zn^{2+}, and Ni^{2+} ions with aqueous solutions of poly(ethylene oxide).[59] Since CdS grows with a superlattice morphology and PbS does not, a strong oligoethylene oxide−cation interaction is not the key factor in direct templating.

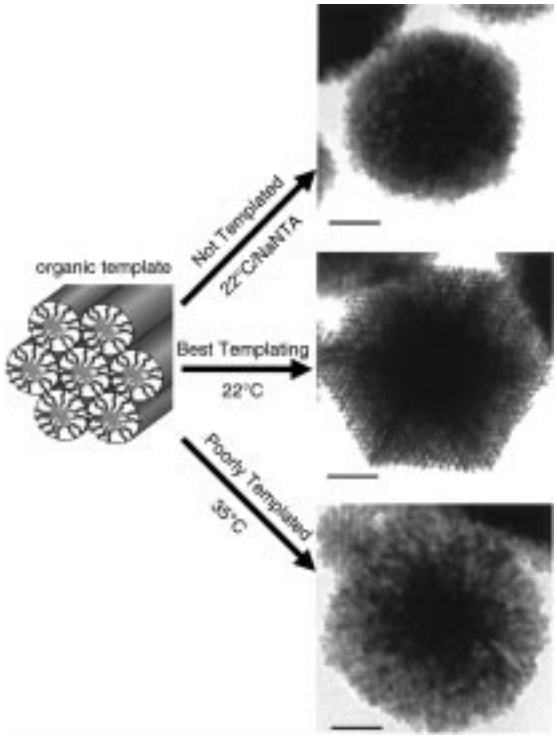

Figure 8. Schematic representation of the hexagonal mesophase and TEM images demonstrating the result of various mineralization conditions (bar = 50 nm). The addition of nitrilotriacetic acid trisodium salt (NaNTA) to the mesophase results in the precipitation of particles with no periodic nanostructure (top). Poorly ordered product is obtained if the mineralization is carried out at an elevated temperature of 35 °C (bottom). The best templating is obtained when the mesophase is not destabilized by heat and the cations are not chelated (middle).

The precipitations at elevated temperature also offer some insight on the formation of morphologically templated solids. As previously discussed, the periodically nanostructured solids are thermodynamically stable relative to the respective nonfeatured metal sulfides in the mesophases studied. This implies there is a critical energy balance between the reduction of surface area in the mineral phase and disruption of the mesophase by the growth of unfeatured mineral. To study this further, we precipitated CdS in mesophases at both 35 and 50 °C. These temperatures are both below the isotropization temperature of the doped mesophases, so the reactions were still carried out in self-assembled media. The CdS produced from the reaction at 35 °C does express the order of the mesophase but poorly compared with the order obtained in the room temperature precipitation (22 °C) (Figure 8). The precipitation at 50 °C, on the other hand, resulted in mineral without a periodic nanostructure. These experiments suggest that the energy difference is small between the periodically nanostructured solid and the bulk metal sulfide.

The periodic nanostructure characteristic of the templated solids was not observed in several metal sulfides such as Ag_2S, CuS, HgS, and PbS irrespective of counterion. There are several chemical differences between the nanostructured systems and systems with no observable nanostructure (see Table 1). Electron diffraction patterns were obtained from all the mineralized particles synthesized, and then the crystal structures were determined comparing the patterns with those in the JCPDS-ICDD powder diffraction file for each mineral. In all cases, the crystal structures were the same for the minerals grown from either the acetate or the nitrate precursors. All of the nanostructured systems had the wurtzite crystal structure (space group

(55) West, T. S. *Complexomety with EDTA and Related Reagents*, 3rd ed.; BDH Chemical Ltd.: Poole, 1969.
(56) Cotton, F. A.; Wilkinson, G. *Advanced Inorganic Chemistry*, 5th ed.; Cotton, F. A., Wilkinson, G., Eds.; John Wiley & Sons: New York, 1988; p 743.
(57) Shewmon, P. *Diffusion in Solids*, 2nd ed.; The Minerals, Metals & Materials Society: Warrendale, PA, 1989.
(58) *CRC Handbook of Chemistry and Physics*, 78th ed.; Lide, D. R., Ed.; CRC Press: New York, 1997; pp 5−93.
(59) Wendsjo, A.; Thomas, J. O.; Lindgren, J. *Polymer* **1993**, 34, 2243.

Table 1. Crystal Structure and Electronegativity Differences of Metal Sulfides and Selenides

mineral	observed crystal structure	Pauling's electronegativity difference between metal and sulfur (selenium)
CdS	*P*63*mc* (wurtzite)	0.89
CdSe	*P*63*mc* (wurtzite)	0.82
ZnS	*P*63*mc* (wurtzite)	0.93
Ag_2S	*P*21/*n* (acanthite)	0.65
CuS	*P*63/*mmc* (covellite)	0.68
HgS	*F*-43*m* (sphalerite)	0.58
PbS	*F*3*m*3 (zincblend)	0.25

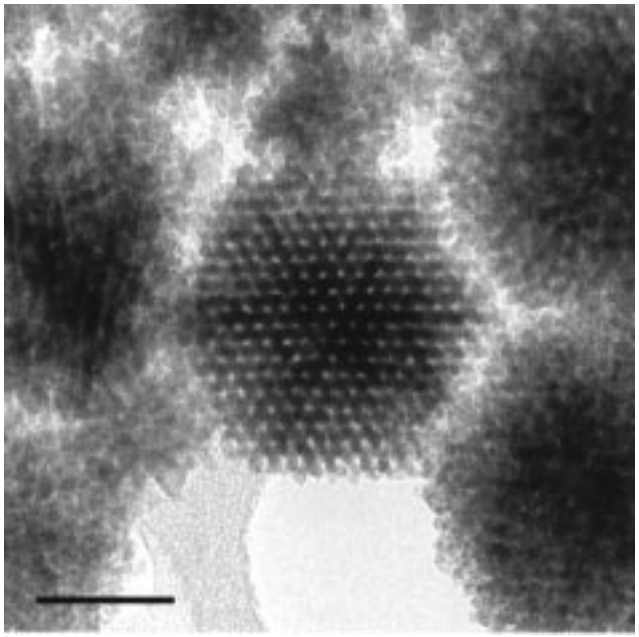

Figure 9. TEM image of $Cd_{0.5}Zn_{0.5}S$ grown from a hexagonal mesophase doped with 0.05 M $Cd(NO_3)_2$ and 0.05 M $Zn(NO_3)_2$ (bar = 50 nm).

*P*63*mc*), while the other systems had a variety of crystal structures. The crystal structure is, of course, related to the relative size of the ions and their electronegativity difference. Furthermore, the electronegativity difference between the metal and sulfur ions may also be a key element in direct templating. The templated materials have a high electronegativity difference, while those with a smaller difference were not nanostructured. PbS (the most covalent of the minerals grown) formed large, cube-shaped single crystals in the mesophase while the less covalent systems (Ag_2S, CuS, and HgS) grew as smaller crystallites with less faceting and no observable nanostructure (Figure 1). Only the most ionic systems, those based on CdS and ZnS, are periodically nanostructured and are therefore templated directly by the liquid crystal. One would expect that a greater electronegativity difference between the sulfur and metal would increase the interaction between the polar oligoethylene oxide segments and the growing mineral. This interaction and the presence of trapped template molecules in the mineral pores could reduce the high surface energy of the nanostructured phase.

Binary mixtures of the precursor salts also lead to some very interesting results. In the first case, a hexagonal mesophase containing 0.05 M $Cd(NO_3)_2$ and 0.05 M $Zn(NO_3)_2$ was mineralized. The resulting product ($Cd_{0.5}Zn_{0.5}S$) has a nanostructure that exactly matches that of the template (Figure 9). The system of 0.05 M $Pb(NO_3)_2$ and 0.05 M $Zn(NO_3)_2$ results in a very different nanostructure, consisting of a single crystal

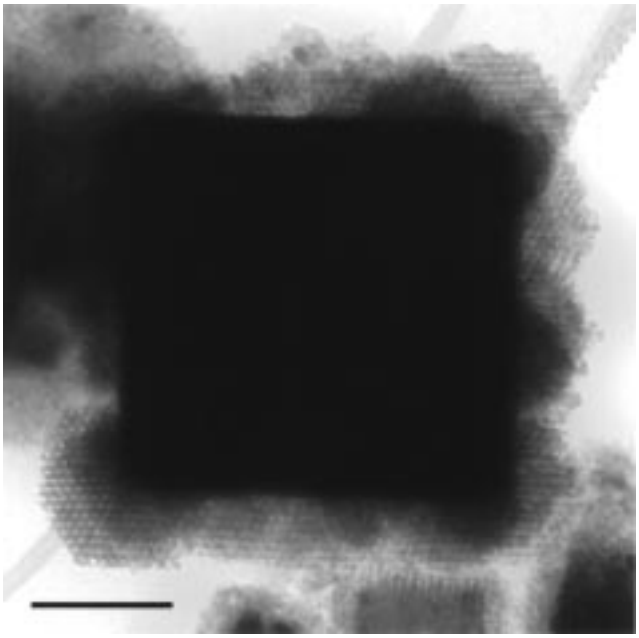

Figure 10. TEM image of a composite product of PbS and ZnS grown in a hexagonal mesophase doped with 0.05 M $Pb(NO_3)_2$ and 0.05 M $Zn(NO_3)_2$. The single crystal cube at the core of the particle is PbS, and the surrounding shell is a periodically nanostructured solid containing ZnS (bar = 100 nm).

core of PbS surrounded by a shell containing nanostructured ZnS (Figure 10). This is effectively the expected result on the basis of the synthesis of single metal sulfides. The formation of mixed metal precipitates gives an insight into the growth processes and also suggests possibilities for property design. The miscible system of $Cd_xZn_{1-x}S$ offers the possibility of band gap engineering, although the somewhat lower solubility of CdS relative to ZnS may lead to particles which are not homogeneous. The significantly different solubility of PbS and ZnS in water plays a very important role in the structure of the particles formed from this mixed system. PbS has a much lower solubility than ZnS, and thus exposure of the doped mesophase to H_2S leads to PbS nucleation. After most of the Pb^{2+} ions are locally depleted, ZnS heterogeneously nucleates on the PbS particles. As expected, the shell containing ZnS is nanostructured.

Conclusions

Direct morphological templating of CdS, CdSe, and ZnS as well as mixed metal systems in a liquid crystal is readily accomplished. The resulting nanostructured materials copy directly the symmetry and dimensions of molecular assemblies in the liquid crystal. To date, both hexagonal and lamellar nanostructures have been generated with periodicities ranging from 7 to 10 nm, depending on synthetic conditions. Since the symmetry and lattice constant of the mineralized superlattice are directly controlled by the liquid crystal, the structure of the product can be designed through the templating mesophase. Through a variety of experiments, the superlattice morphology of the nanostructured systems was found to be thermodynamically stable in contact with mesophase with respect to the solid materials without morphological order. The phenomenon of direct templating using the methodology outlined here is chemically specific as demonstrated by its failure in Ag_2S, CuS, HgS, and PbS. When these minerals are grown in hexagonal or lamellar mesophases, they do not contain any features commensurate with the precursor liquid crystal's symmetry and dimensions. We specifically hypothesize that templating requires

favorable interaction between the amphiphile and the resulting mineralized structure.

Experimental Section

Materials. Unless otherwise noted, all reagent grade chemicals were used as received, and deionized water was used throughout. The amphiphile $(EO)_{\overline{10}}$oleyl was obtained from ICI Surfactants (Wilmington, Delaware). It has an average degree of polymerization of 10 ethylene oxide structural units in its hydrophilic segment and an oleyl hydrophobic segment. H_2S gas was saturated with water by passing through an aerator before entering the reaction flask.

Sulfide Synthesis. All sulfides were synthesized by the reaction of hydrogen sulfide gas (H_2S) with the appropriate metal salt using the lyotropic aqueous mesophase as a template. The mesophase was formed by mixing the amphiphile with an aqueous salt solution, adjusting the volume ratio to yield the desired type of molecular order. Unless otherwise stated, precipitations were carried out at room temperature in a hexagonal mesophase formed using equal volumes of amphiphile and 0.1 M aqueous salt solutions. However, silver acetate was used in a concentration of 0.05 M because of its limited solubility. In all experiments, both components of the mesophase were combined in a vial and mixed above the system's isotropization temperature for a few minutes and then allowed to cool to room temperature. The mercury salts were not stable unless the water and amphiphile were degassed prior to use and air was excluded from the system (otherwise a white precipitate rapidly formed). The diffusion of H_2S into the mesophase rapidly starts the conversion of the salt to the metal sulfide and byproduct (acetic or nitric acid). After the reaction was complete, the resulting metal sulfide−mesophase composite was washed three times to remove byproducts and unbound amphiphile. Each washing involved dispersing the material in a 50:50 vol % solution of diethyl ether/ethanol via sonication, followed by centrifugation and removal of the clear supernatant.

Selenide Synthesis. Hydrogen selenide (H_2Se) was generated by the addition of water or a dilute solution of sulfuric acid to Al_2Se_3 which had been prepared from the elements shortly prior to use.[60] Typically, water was added first, and when gas evolution slowed dilute sulfuric acid was added. The H_2Se was then flowed over a mesophase prepared with either 0.1 M $Cd(OAc)_2$ or 0.025 M $Cd(NO_3)_2$, generating CdSe and acid byproduct.[61] The mesophase preparation and post precipitation washing sequences were identical to those in the sulfide synthesis.

Electron Microscopy. Transmission electron microscopy was performed on a Philips CM 12 or CM 200 instrument operating at 120 kV. Samples were prepared by dispersing the powders in ethanol and evaporating a drop of this suspension on a holey carbon-coated copper grid.

Liquid Crystal Phase Determination. Phases were identified by X-ray diffraction and textures observed with polarized optical microscopy (POM). The X-ray diffractograms of the mesophase were collected on a Siemens SAXS machine with a nickel-filtered copper rotating anode source and an area detector. POM was performed using a Leitz Laborlux 12 POL optical polarized microscope with a Linkham THM 600 hotstage. The samples were heated above their isotropization temperature and air cooled before X-ray diffractograms were collected in order to remove any orientation effects from sample preparation. POM samples were made by sandwiching the mesophase between two glass slides, heating it above its isotropization temperature, and then cooling at 10 °C/min to room temperature. The phase diagram was determined for samples with an amphiphile content ranging from 25 to 90 vol %. For homogeneity, each sample was well mixed above its isotropization temperature and allowed to stand at room temperature overnight prior to characterization.

Nuclear Magnetic Resonance. Nuclear Magnetic Resonance (NMR) studies were carried out using a General Electric QE300 (7.05 T). Both doped and undoped mesophases were prepared in 10 mm NMR tubes containing equal volumes of deuterium oxide and amphiphile (mixed and annealed as previously described).

Mesophase Fractionation. To investigate the growth mechanism and size distribution of CdS particles generated from a hexagonal mesophase doped with $Cd(NO_3)_2$, we precipitated CdS in a plastic vial (containing approximately 3 cm of hexagonal mesophase). The gel-like mesophase was then cut into 2 mm thick disks whose faces were parallel to the top of the vial. Each section was separately washed as previously described to yield precipitate with a well-defined exposure time to H_2S (between 0 and 15 h, depending on the section depth).

Effect of Binding Agent on the Synthesis of CdS. Mesophases were formed from a solution of either 0.05 M $Cd(OAc)_2$ or 0.05 M $Cd(NO_3)_2$, in addition to 0.05 M NaNTA and an equal volume of the amphiphile. Another hexagonal mesophase was prepared from a solution of 0.05 M $Cd(OAc)_2$, 0.8 M NH_3, and the amphiphile. These systems all became irreversibly opaque if heated and were therefore generated by alternately adding amphiphile and aqueous solutions dropwise to a vial, followed by several days of equilibration (yielding a homogeneous mesophase). CdS was precipitated and worked up by the standard method.

Relative Diffusion Rates of H_2S and Aqueous Salts. The relative diffusivities of aqueous 0.1 M salts and H_2S within the hexagonal mesophases were determined by filling a vial with 10 mm of mesophase doped with 0.1 M $Cd(OAc)_2$ or 0.1 M $Pb(OAc)_2$. The vial was cooled close to 0 °C, and another 10 mm of a hot (isotropic) solution of 50 vol % H_2O and 50 vol % amphiphile was added. This vial rapidly cooled to room temperature, and then H_2S gas was allowed to flow over it.

Acknowledgment. This work was supported in part by the U.S. Department of Energy, Division of Materials Science Grant DEFG02-96ER45439, through the University of Illinois at Urbana-Champaign, Frederick Seitz Materials Research Laboratory, and by a grant from the Department of Energy Center of Excellence for the Synthesis and Processing of Advanced Materials. The authors acknowledge the Beckman Institute for Advanced Science and Technology for a graduate fellowship granted to P.V.B.

JA9833725

(60) Waitkins, G. R.; Shutt, R. *Inorg. Synth.* **1946**, *2*, 184.

(61) H_2Se is highly toxic, and so was only generated as required. All steps were performed in a fume hood to prevent accidental exposure.